INT-PUB-10-033

Influence of vector interaction and Polyakov loop dynamics on inhomogeneous chiral symmetry breaking phases

Stefano Carignano[1], Dominik Nickel[2], and Michael Buballa[1]
[1]*Institut für Kernphysik, Technische Universität Darmstadt, Germany*
[2]*Institute for Nuclear Theory, University of Washington, Seattle, USA*
(Dated: July 2010)

We investigate the role of the isoscalar vector interaction and the dynamics of the Polyakov loop on inhomogeneous phases in the phase diagram of the two-flavor Nambu-Jona–Lasinio (NJL) model. Thereby we concentrate on inhomogeneous phases with a one-dimensional modulation, explicitly domain-wall solitons and, for comparison, the chiral spiral. While the inclusion of the Polyakov loop merely leads to quantitative changes compared to the original NJL model, the inclusion of a repulsive vector-channel interaction has significant qualitative effects: Whereas for homogeneous phases the first-order phase transition gets weakened and eventually turns into a second-order transition or a cross-over, the domain of inhomogeneous phases is less affected. In particular the location of the Lifshitz point in terms of temperature and density is not modified. Consequently, the critical point disappears from the phase diagram and only a Lifshitz point (showing a different critical behavior) remains. In particular, susceptibilities remain finite.

I. INTRODUCTION

Due to its potentially rich and complex structure a better understanding of the phase diagram of quantum chromodynamics (QCD) still poses one of the biggest challenges in modern nuclear physics (for dedicated reviews see, e.g., Refs. [1–3]). Experimentally, the domain of large temperatures is explored by heavy-ion collisions whereas the properties at low temperatures and large densities are relevant for compact stellar objects. On the theoretical side ab-initio lattice calculations are limited to small chemical potentials and investigations at moderate densities so far mainly rely on phenomenological models. Probably the most widely-used one in this context is the Nambu-Jona–Lasinio (NJL) model [4] and its extensions, sharing global symmetries as well as the phenomenon of chiral symmetry breaking with QCD (see Refs. [5–8] for reviews).

In this article we explore the role of inhomogeneous phases in the phase diagram of NJL-type models, focusing on the inclusion of a vector-channel interaction as well as the Polyakov-loop dynamics. The isoscalar-vector interaction naturally arises in the NJL model when motivating the interaction from a one-gluon exchange in QCD [5] and was already shown to be of particular importance in the Walecka model at finite densities [9]. More recently, its influence on the location and emergence of critical points in the phase diagram has attracted new interest [10–12].

The coupling of the NJL model to the Polyakov-loop dynamics on the other hand has been introduced to mimic features of (de-)confinement, in particular at finite temperatures and vanishing densities [13, 14]. There are several open issues which complicate the setup of the model at finite chemical potential [15, 16]. However, at vanishing temperatures, the Polyakov loop always decouples from the quark sector by construction. In the regime of low temperatures and (not too) high

chemical potential one typically finds a chirally restored but "confined" phase, which is sometimes related to the quarkyonic phase [17], suggested in Ref. [18] for QCD in the limit of a large number of colors (N_c).

Although most studies are usually restricted to homogeneous phases, the importance of chiral crystalline phases being characterized by an inhomogeneous order parameter has been pointed out long ago. Well known examples are the Skyrme crystal [19] and the chiral density wave (CDW) [20]. For quark matter, chiral crystalline phases have been explored in the weakly coupled regime for large N_c [21, 22], where they form the ground state at vanishing temperatures even at asymptotic densities. Related to that they naturally show up in the quarkyonic matter picture [23] and in holographic models [24]. For metals, however, the underlying mechanism of particle-hole pairing was however already considered in the 1960s [25]. In a similar context inhomogeneous phases have also been discussed for color superconductivity, see e.g. Refs. [26–32], again borrowing ideas from condensed matter physics [33, 34].

An inhomogeneous phase also exists in the large N_c-limit of the $1+1$-dimensional Gross-Neveu (GN) model [35], where one has a rather complete picture of the phase diagram [36–39]. Here the chiral crystalline phase emerges at low densities by formation of kink and antikink solitons and reaches out to arbitrarily high densities for sufficiently small temperatures.

In the NJL model, most investigations of inhomogeneous phases have been performed for the CDW ("chiral spiral"), corresponding to a single plane wave ansatz for the order parameter [40, 41]. The notable exception here is Ref. [42]. More recently, it was shown that the known solutions from the $1+1$-dimensional GN model can be used to construct solutions of the $3+1$ dimensional NJL model whose order parameter varies in one spatial direction [43]. These solutions are more favored than the chiral spirals and the corresponding phase occupies a larger region of the phase diagram. However, due to the short-ranged interaction (in contrast to the weak-coupling QCD analysis at large N_c) and different kinematics compared to the GN model, this phase is constrained to a finite range of densities.

In the chiral limit, we can thus distinguish three different phases, namely the homogeneous chirally broken phase, the inhomogeneous phase, and the chirally restored phase. These phases meet in a single point, a so-called "Lifshitz point" (LP). Within a Ginzburg-Landau analysis it can be shown that in the NJL model without vector interactions the LP exactly coincides with the (tri-) critical point (CP) of the chiral phase transition, which would be present if the analysis was limited homogeneous phases [44]. In Ref. [43] this was confirmed by an explicit model calculation. Moreover, it was found that the inhomogeneous phase is bordered by second-order phase boundaries, and that it completely covers the would-be first-order transition line between the homogeneous phases.

In the present work we extend these investigations to include repulsive vector interactions. As the main result we find that the LP stays at the same temperature, whereas, when the analysis is restricted to homogeneous phases, the CP is shifted to smaller temperatures and larger chemical potentials. The critical region surrounding the CP thus disappears from the phase diagram as it is replaced by an energetically more preferred inhomogeneous ground state. Consequently, the divergence of susceptibilities at the CP, which has been related to event-by-event fluctuations in heavy-ion collisions and discussed as one of the most important experimental signatures of the

CP [45], is removed from the phase diagram. For completeness, we also discuss the inclusion of the Polyakov-loop dynamics, which affects the structure of the phase diagram only quantitatively.
This paper is organized as follows: In section II we discuss the role of the isoscalar-vector interaction when investigating the NJL model's phase diagram allowing for inhomogeneous phases. After introducing the model and the general framework for investigating inhomogeneous phases in subsections II A and II B, respectively, we move on to an extensive numerical study of the phase diagram in subsection II C. The latter includes results for the density profiles in solitonic ground states, a comparison to the CDW, a discussion of number susceptibilities and the role of finite current quark masses. Part of the obtained results is then explained in the context of a generalized Ginzburg-Landau (GL) expansion in subsection II D. The subsequent section III is devoted to the inclusion of Polyakov loop dynamics and its effect on the structure of the phase diagram. Finally, we summarize and conclude in section IV.

II. THE TWO-FLAVOR NJL MODEL WITH VECTOR-CHANNEL INTERACTION

A. Model and Approximations

In view of finite density investigations, an important extension of the original NJL model is given by the inclusion of an isoscalar vector-channel interaction. The Lagrangian is then given by

$$\mathcal{L} = \bar{\psi}\left(i\gamma^\mu\partial_\mu - m\right)\psi + G_S\left(\left(\bar{\psi}\psi\right)^2 + \left(\bar{\psi}i\gamma^5\tau^a\psi\right)^2\right) - G_V\left(\bar{\psi}\gamma^\mu\psi\right)^2 , \tag{1}$$

where ψ is a $4N_fN_c$-dimensional quark spinor for $N_f = 2$ flavors and $N_c = 3$ colors, γ^μ and τ^a are Dirac and Pauli matrices, respectively, and m is the degenerate current quark mass.
In mean-field approximation we expand around the expectation values of the non-vanishing, potentially spatially varying scalar condensate $S(\mathbf{x}) \equiv \langle\bar{\psi}(\mathbf{x})\psi(\mathbf{x})\rangle$, pseudo-scalar condensate $P_3(\mathbf{x}) \equiv \langle\bar{\psi}(\mathbf{x})\, i\gamma^5\tau^3\psi(\mathbf{x})\rangle$ and density $n(\mathbf{x}) \equiv \langle\psi^\dagger(\mathbf{x})\psi(\mathbf{x})\rangle$, yielding

$$\begin{aligned}
(\bar{\psi}\psi)^2 &\simeq -S(\mathbf{x})^2 + 2S(\mathbf{x})\bar{\psi}\psi\,,\\
(\bar{\psi}i\gamma^5\tau^a\psi)^2 &\simeq -P(\mathbf{x})^2 + 2P(\mathbf{x})\bar{\psi}i\gamma^5\tau^3\psi\,,\\
(\bar{\psi}\gamma^\mu\psi)^2 &\simeq -n(\mathbf{x})^2 + 2n(\mathbf{x})\bar{\psi}\gamma^0\psi\,.
\end{aligned} \tag{2}$$

In the case of a periodic condensate with Wigner-Seitz cell V and using the imaginary-time formalism, the mean-field thermodynamic potential is then given by

$$\begin{aligned}
\Omega &= -\frac{T}{V}\ln\int\mathcal{D}\bar{\psi}\mathcal{D}\psi\exp\left(\int_{x\in[0,\frac{1}{T}]\times V}\left(\mathcal{L}_{\mathrm{mean-field}} + \mu\bar{\psi}\gamma^0\psi\right)\right)\\
&= \Omega_{\mathrm{kinetic}} + \Omega_{\mathrm{cond}}\,,
\end{aligned} \tag{3}$$

with the individual contributions

$$\begin{aligned}
\Omega_{\mathrm{kinetic}} &= -\frac{T}{V}\sum_n \mathrm{Tr}_{D,c,f,V}\,\ln\left(\frac{1}{T}\left(i\omega_n + H - \mu\right)\right)\,,\\
\Omega_{\mathrm{cond}} &= \frac{1}{V}\int d\mathbf{x}\left(\frac{|M(\mathbf{x}) - m|^2}{4G_S} - \frac{(\tilde{\mu}(\mathbf{x}) - \mu)^2}{4G_V}\right)\,,
\end{aligned} \tag{4}$$

the quasi-particle Hamiltonian

$$H-\mu \;=\; \underbrace{-i\gamma^0\gamma^i\partial_i + \frac{\gamma^0}{2}\left(M(\mathbf{x}) + M(\mathbf{x})^* + \gamma^5\tau^3 M(\mathbf{x}) - \gamma^5\tau^3 M(\mathbf{x})^*\right)}_{\equiv H_0} - \tilde{\mu}(\mathbf{x})\,, \tag{5}$$

the spatially dependent "constituent quark" mass

$$M(\mathbf{x}) = m - 2G_s(S(\mathbf{x}) + iP(\mathbf{x}))\,, \tag{6}$$

the renormalized quark chemical potential

$$\tilde{\mu}(\mathbf{x}) = \mu - 2G_V\, n(\mathbf{x})\,, \tag{7}$$

and Matsubara frequencies $\omega_n = (2n+1)\pi T$.

For general spatially dependent mean fields, the evaluation of the functional trace in Eq. (4) and the subsequent minimization of Ω is highly non-trivial. However, as shown in Ref. [43], for the case without vector interactions a solution can be found if only one-dimensional mass modulations are considered. In the present work we want to generalize these solutions to $G_V > 0$. Since this cannot be done exactly in a straightforward manner, we approximate the density in Eq. (7) by its spatial average,

$$n(\mathbf{x}) \;\to\; \bar{n} \;\equiv\; \langle n(\mathbf{x})\rangle \;=\; \text{const.} \tag{8}$$

As a consequence, $\tilde{\mu}$ becomes constant as well, and the problem reduces to the known case without vector interaction at a shifted value of the chemical potential. Of course, at first sight, it seems rather questionable whether the replacement Eq. (16) is a good approximation in an inhomogeneous phase. However, as we will discuss in more detail later on, it can be rigorously justified in the vicinity of a second-order phase boundary to the restored phase, and in particular for the Lifshitz point.

The kinetic contribution Ω_{kinetic} to the thermodynamic potential can now be evaluated from the eigenvalue spectrum $\{E_i\}$ of the Hamiltonian H_0 through the relation

$$T\sum_n \ln\left(\frac{1}{T}(i\omega_n + E_i)\right) \;=\; \frac{1}{2}E_i + T\ln\left(1+\exp\left(-\frac{E_i}{T}\right)\right)\,. \tag{9}$$

Introducing a density of states to express $-\frac{1}{2V}\sum_{E_i} \to -2N_c\int dE\,\rho(E)$, we then formally obtain

$$\Omega_{\text{kinetic}} \;=\; -2N_c\int_0^\infty dE\,\rho(E)\,f(E)\,, \tag{10}$$

with

$$\begin{aligned} f(E) \;&=\; f_{\text{UV}}(E) + f_{\text{thermal}}(E)\,,\\ f_{\text{UV}}(E) \;&=\; E\,,\\ f_{\text{thermal}}(E) \;&=\; T\,\ln\left(1+\exp\left(-\frac{E-\tilde{\mu}}{T}\right)\right) + T\,\ln\left(1+\exp\left(-\frac{E+\tilde{\mu}}{T}\right)\right)\,, \end{aligned} \tag{11}$$

where we have used the fact that the eigenvalues of H_0 come in pairs $\{E_i, -E_i\}$.
The last missing step is a regularization of the diverging integration. For homogeneous phases this is mostly done by a momentum cutoff (see, e.g., Refs. [5–8]). This is however not possible for inhomogeneous phases, since the quasi-particle energies can no longer be labelled by a conserved three-momentum. Instead we have to apply a regularization of the functional logarithm, e.g., by a proper-time regularization, which essentially acts on the energy spectrum rather than the quasi-particle momenta. With the density of states growing like $\rho(E) = E^2/\pi^2 + O(E^0)$ in three dimensions, we then only have to regularize the contribution at $T = \tilde{\mu} = 0$ stemming from $f_{\rm UV}(E)$. We regularize this part by a specific blocking function in the proper-time integral leading to a Pauli-Villars regularization of the form [6]

$$f_{\rm UV}(E) \;\to\; f_{\rm PV}(E) \;=\; \sum_{j=0}^{3} c_j \sqrt{E^2 + j\Lambda^2}\,, \tag{12}$$

with $c_0 = 1$, $c_1 = -3$, $c_2 = 3$, $c_3 = -1$ and a cutoff scale Λ.
Within this setup we aim to discuss ground states by considering the stationary conditions

$$\frac{\delta\Omega}{\delta M(\mathbf{x})} \;=\; 0\,, \tag{13}$$

$$\frac{\partial\Omega}{\partial\tilde{\mu}} \;=\; 0\,, \tag{14}$$

determining the order parameter $M(\mathbf{x})$ and the shifted chemical potential $\tilde{\mu}$. We recall that the latter is a space-independent constant after inserting our approximation Eq. (8) into Eq. (7). For the later discussion it is helpful to cast condition (14) into

$$\mu \;=\; \tilde{\mu} + 2G_V\,\bar{n}\,, \tag{15}$$

where the average density is given by

$$\bar{n} \;=\; 2N_c \int_0^\infty dE\,\rho(E)(n_+ - n_-) \tag{16}$$

with the occupation numbers $n_\pm = 1/(1+\exp((E\mp\tilde{\mu})/T))$. We emphasize that, besides explicitly depending on $\tilde{\mu}$ via the occupation numbers, $\bar{n}$ is a functional of $M(\mathbf{x})$ via the density of states $\rho(E)$.
At this stage it is worth noting that for most quantities all dependence on G_V can be absorbed into $\tilde{\mu}$. In particular the form of the gap equation (13) and, hence, its solutions $M(\mathbf{x})$ are identical to the case without vector interaction upon replacing $\mu \to \tilde{\mu}$. As obvious from Eq. (16), the same is true for the average density $\bar{n}$. As a consequence, the mass functions $M(\mathbf{x})$ at a given $\bar{n}$ do not depend on G_V. For homogeneous phases this is a well-known result [8]. The remaining effect of G_V is on the one hand side to map $\tilde{\mu}$ onto μ via Eq. (15), and on the other hand to shift the value of the thermodynamic potential of a solution by $-G_V\bar{n}^2$. This will be important for the explanation of our results later on.

B. One-dimensional modulations

For the explicit evaluation of the expressions derived in Sec. II A we still need to determine the density of states $\rho(E)$. In general, for arbitrary mass functions $M(\mathbf{x})$, this is highly non-trivial and the problem gets even more involved for the subsequent variation in $M(\mathbf{x})$. However, as mentioned earlier, if we restrict ourselves to phases with one-dimensional modulations the task can be reduced to a problem in the $1+1$-dimensional GN model [43]. Since furthermore for the GN model all inhomogeneous phases have been classified [46] and in particular the phase diagram has been discussed in detail [36–39], the investigation of these phases simplifies strongly.

In the following we always assume that the one-dimensional modulations are in z-direction, i.e., the system is invariant under translations in the xy-directions. In the chiral limit the favored mass functions then take the form[1]

$$M_{\text{soliton}}(\mathbf{x}) = \nu\Delta\,\frac{\text{sn}(\Delta z|\nu)\text{cn}(\Delta z|\nu)}{\text{dn}(\Delta z|\nu)}\,, \tag{17}$$

where sn, cn, and dn are Jacobi elliptic functions, and ν and Δ are two independent parameters. $M_{\text{soliton}}(\mathbf{x})$ parameterizes a lattice of domain-wall solitons. For $\nu \to 1$ this solution becomes thermodynamically degenerate with a homogeneous phase, since this limit corresponds to a single soliton localized around $z = 0$, which does not contribute in the thermodynamic limit.

The density of states in this phase is explicitly given by [43]

$$\begin{aligned}\rho_{\text{soliton}}(E) = \frac{E\Delta}{\pi^2}\Bigg\{ &\quad \theta(\sqrt{\tilde\nu}\Delta - E)\left[\mathbf{E}(\tilde\theta|\tilde\nu) + \left(\frac{\mathbf{E}(\nu)}{\mathbf{K}(\nu)} - 1\right)\mathbf{F}(\tilde\theta|\tilde\nu)\right] \\ &+\ \theta(E - \sqrt{\tilde\nu}\Delta)\theta(\Delta - E)\left[\mathbf{E}(\tilde\nu) + \left(\frac{\mathbf{E}(\nu)}{\mathbf{K}(\nu)} - 1\right)\mathbf{K}(\tilde\nu)\right] \\ &+\ \theta(E-\Delta)\left[\mathbf{E}(\theta|\tilde\nu) + \left(\frac{\mathbf{E}(\nu)}{\mathbf{K}(\nu)} - 1\right)\mathbf{F}(\theta|\tilde\nu) + \frac{\sqrt{(E^2-\Delta^2)(E^2-\tilde\nu\Delta^2)}}{E\Delta}\right]\Bigg\}\,,\end{aligned} \tag{18}$$

where $\mathbf{K}$ and $\mathbf{F}$ are the complete and incomplete elliptic integrals of 1st kind, respectively, and $\mathbf{E}$ are the (complete or incomplete) elliptic integrals of 2nd kind. Furthermore we introduced the notations $\tilde\nu = 1-\nu$, $\tilde\theta = \arcsin(E/(\sqrt{\tilde\nu}\Delta))$, and $\theta = \arcsin(\Delta/E)$.

With these expressions at hand, the stationary condition (13) for the ground state of the system is reduced from a complicated functional derivative to the much simpler problem of extremizing the thermodynamic potential in the two parameters Δ and ν. As argued in Ref. [43] the solutions obtained by extremizing the thermodynamic potential in the remaining parameters then also fulfill the more general stationary condition (13).

We can also consider finite current quark masses, for which the order parameter is generalized to

$$M_{\text{soliton,m}}(z) \;=\; \Delta\left(\nu\,\text{sn}(b|\nu)\text{sn}(\Delta z|\nu)\text{sn}(\Delta z + b|\nu) + \frac{\text{cn}(b|\nu)\text{dn}(b|\nu)}{\text{sn}(b|\nu)}\right)\,. \tag{19}$$

[1] This expression can be rewritten as $M_{\text{soliton}}(\mathbf{x}) = \sqrt{\nu'}\Delta'\,\text{sn}(\Delta' z|\nu')$ where $\nu' = (\frac{1-\sqrt{1-\nu}}{1+\sqrt{1-\nu}})^2$ and $\Delta' = (1+\sqrt{1-\nu})\Delta$, but Eq. (17) is more convenient for our purpose.

Here b is an additional parameter to be varied together with Δ and ν. The density of states changes to

$$\rho_{\mathrm{soliton,m}}(E) \;=\; \frac{E}{\sqrt{E^2-\delta\Delta^2}}\rho_{\mathrm{soliton}}(\sqrt{E^2-\delta\Delta^2})\theta(E-\sqrt{\delta}\Delta)\,, \tag{20}$$

where $\delta \in [0,\infty]$ is given by $\mathrm{sn}(b|\nu) = \frac{1}{\sqrt{1+\delta}}$. The chiral limit, i.e. $m = 0$, corresponds to $\delta = 0$ or equivalently $b = \mathbf{K}(\nu)$.
For comparison we will sometimes also consider the chiral density wave (CDW or "chiral spiral") defined by the mass function

$$M_{\mathrm{CDW}}(\mathbf{x}) = \Delta \exp(iqz)\,. \tag{21}$$

In this case we restrict ourselves to the chiral limit and the corresponding density of states is given by [43]

$$\begin{aligned}\rho_{CDW}(E) = \frac{E}{2\pi^2}\Big\{ \quad & \theta(E-q-\Delta)\sqrt{(E-q)^2-\Delta^2} \\ + \;& \theta(E-q+\Delta)\theta(E+q-\Delta)\sqrt{(E+q)^2-\Delta^2} \\ + \;& \theta(q-\Delta-E)\left(\sqrt{(E+q)^2-\Delta^2}-\sqrt{(E-q)^2-\Delta^2}\right)\Big\}\,.\end{aligned} \tag{22}$$

In the NJL model, however, the CDW is always less favored than the soliton lattice. The main reason to include it in our discussion is its simplicity. In particular its density profile is uniform. This is most easily seen by applying a global chiral transformation of the form $\psi \to \exp(i\gamma_5\tau_3\, qz_0/2)\psi$ with some constant z_0. While the density $\langle\psi^\dagger(\mathbf{x})\psi(\mathbf{x})\rangle$ is invariant under this transformation, it leads to a phase shift in $M(x)$ which is equivalent to a translation by z_0 in the z-direction. Hence the density must be uniform. The replacement Eq. (8) is therefore an exact manipulation for the CDW, which will allow us to comment on the corresponding approximation for the solitons.

C. Numerical results including the vector-channel interaction

Having set up the formalism for the inclusion of the vector interaction, we now turn to the numerical part of our investigations. As in Ref. [43] we fix the parameters in the chiral limit by requiring for the pion decay constant $f_\pi = 88$ MeV and for the constituent mass in the vacuum $M_0 = 300$ MeV. The resulting parameter values are $\Lambda = 757.0$ MeV and $G_S = 6.002/\Lambda^2$. The value of G_V, on the other hand, is treated as a free parameter, which will be varied in order to study its effect on the phase diagram. Starting from a color-current interaction and performing a Fierz transformation one would get $G_V/G_S = 1/2$, whereas fits to the vector meson spectrum typically yield larger values [5, 47]. In the following we will therefore vary G_V between zero and G_S. In particular we will restrict ourselves to repulsive vector interactions, similar as in the Walecka model.

1. Phase diagrams in the chiral limit

Probably the most interesting result of this work is the effect of the vector-channel interaction on the transition lines in the phase diagram. In Fig. 1 we present the $\mu - T$ phase diagrams for

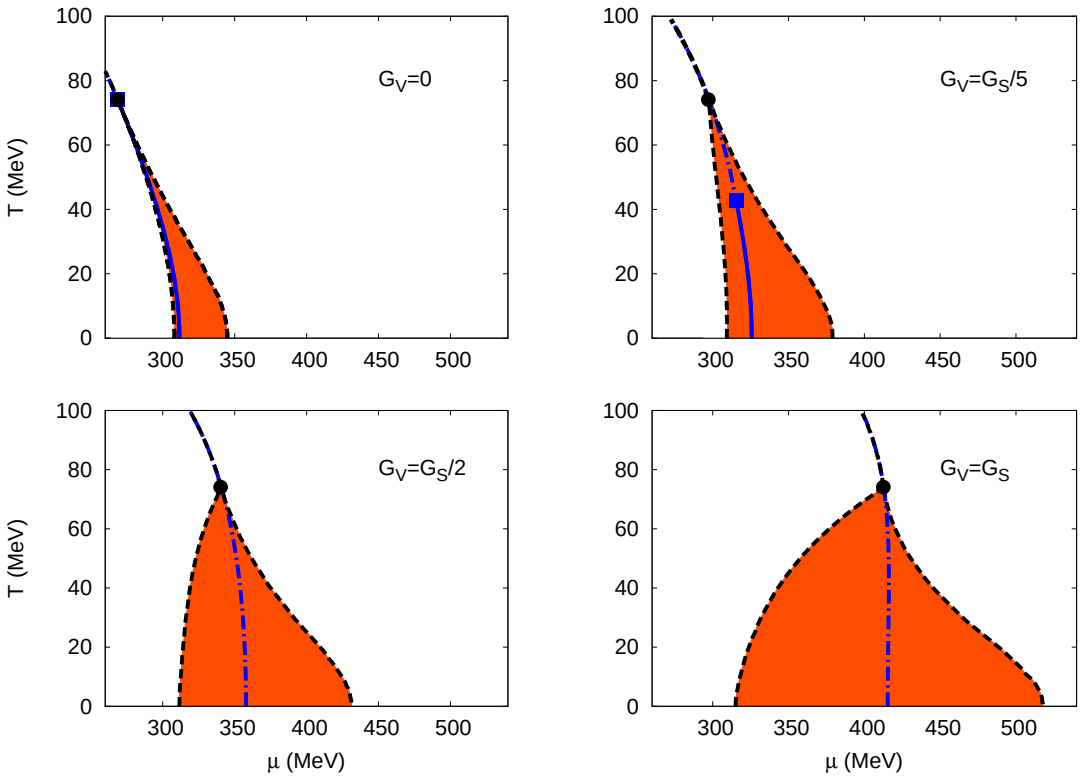

FIG. 1: The phase diagram in the chiral limit for different values of the vector coupling when allowing for the domain-wall soliton lattice. The black dashed lines represent the second-order transition lines joining at the Lifshitz point (dot), the shaded region represents the inhomogeneous phase. The blue solid lines represent the first-order phase transition obtained when limiting to homogeneous order parameters, which turns to second order (blue dot-dashed lines) at the critical point (square).

various values of G_V, focusing on the region where the domain-wall soliton lattice is preferred. The calculations have been performed in the chiral limit. For comparison we have also indicated the transition lines one obtains when the analysis is limited to homogeneous phases. In this case there is a critical point for small values of G_V (blue square) below which the transition from the broken to the restored phase is first order (blue solid line). Upon increasing G_V the CP is shifted to smaller temperatures (and higher chemical potentials) and eventually hits the zero temperature axis, so that the first-order phase transition is absent for larger values of G_V. This behavior is well known [48, 49] and has recently attracted new interest in the discussion of the critical surface [10, 11].

However, the picture changes considerably, when we allow for inhomogeneous solutions. We then always find a regime where the domain-wall solitons are preferred (shaded region), so that we can distinguish three different phases: the homogeneous broken phase, the restored phase and the inhomogeneous phase. The corresponding three phase boundaries are all of second order. Their conjunction defines a Lifshitz point (dot), above which the phase boundary coincides with that found when limiting to homogeneous phases. Moreover, for $G_V = 0$ the LP precisely agrees

with the CP of the purely homogeneous analysis [43, 44]. It turns out, however, that this is no longer true for $G_V > 0$: Whereas with increasing vector coupling the CP moves downwards in temperature and eventually disappears from the phase diagram, we observe that the Lifshitz point is only shifted in the μ-direction, while remaining at the same temperature. Consequently, unlike the first-order boundary in the purely homogeneous case, the existence of the inhomogeneous phase is not inhibited by the vector interaction. At vanishing temperature the transition from the homogeneous broken to the inhomogeneous phase is only slightly varying with G_V, whereas the transition from the inhomogeneous to the restored phase significantly shifts, thus enhancing the domain where inhomogeneous phases are favored.

The observed G_V-dependence of the phase diagram can easily be understood when we recall from the end of section II A that the stationary condition (13) depends on G_V only through $\tilde{\mu}$. Consequently its solutions $M(\mathbf{x})$ at given $(\tilde{\mu}, T)$ are independent of G_V and thus equal to the solutions at $G_V = 0$ where $\tilde{\mu} = \mu$. At $G_V > 0$, we can then translate these solutions into solutions at shifted values of μ, which are obtained from Eq. (15). For a given mass function this mapping is unique since the average density $\bar{n}$, which enters Eq. (15), also depends on G_V only through $\tilde{\mu}$, see Eq. (16).

The consequences of this mapping can be elaborated further for the phase transition lines. We first consider the case of second-order phase transitions as found in our calculation. When approaching the second-order transition from any direction, for each extremum in the thermodynamic potential that is relevant for the transition the density approaches the same value and consequently all extrema are mapped to the same value of μ. Since there is only one extremum left on one side of the phase transition, we only have to make sure that the additional extremum on the other side cannot be mapped beyond the phase transition line, thus generating a spinodal region. For the transitions into the restored phase this is guaranteed by the fact that the restored solution has the highest possible density at given $\tilde{\mu}$ and that the density increases with $\tilde{\mu}$. Therefore no other solution can be mapped beyond the transition line for $G_V > 0$. Similarly the homogeneous broken solution has the lowest density at given $\tilde{\mu}$ and therefore no inhomogeneous solution can be mapped below the transition line when going from the inhomogeneous into the homogeneous broken phase. Consequently all second-order transition lines for $G_V = 0$ are mapped onto second-order transition lines for $G_V > 0$. In particular, this explains why the Lifshitz point stays at the same temperature, as the mapping leaves T untouched.

From the arguments given above, it follows immediately that the phase diagram in the $\tilde{\mu}$-T plane is independent of G_V. Moreover, since in this case $\bar{n}(T, \tilde{\mu})$ is uniquely given by Eq. (16) and therefore also independent of G_V, this means that the $\bar{n}$-T phase diagram is independent of G_V as well. This diagram is presented in Fig. 2.

A slight complication of this picture arises if there is a first-order phase transition at $G_V = 0$, which occurs when limiting to homogeneous phases. In this case we have a spinodal region enclosing the first-order phase transition line, where the thermodynamic potential has several extrema at the same value of μ: two local minima and one local maximum. As before, this means that at $G_V > 0$ we have several solutions at the same value of $\tilde{\mu}$. However, since the local extrema correspond to different masses and therefore to different densities, they will now be mapped onto different values

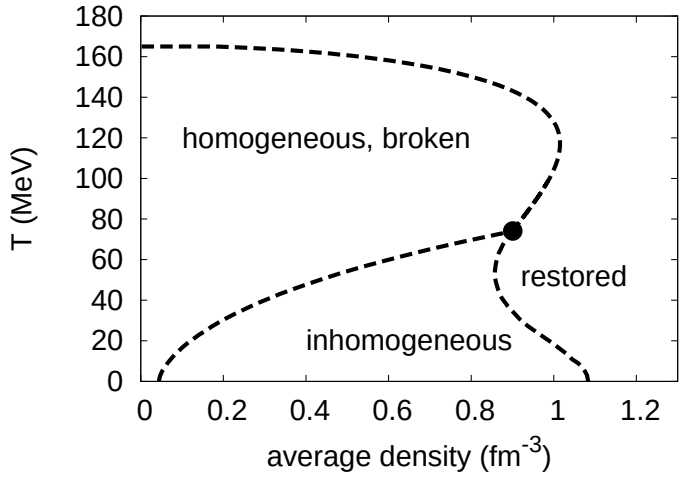

FIG. 2: The phase diagram in the $\bar{n} - T$ plane. The transition lines do not depend on G_V for $G_V > 0$.

of μ by Eq. (15): More precisely, solutions with lower masses will be shifted to higher values of μ than solutions with higher masses. As a consequence, the spinodal region shrinks with increasing G_V, i.e., at fixed temperature the first-order transition gets weakened and eventually becomes second order. This explains why the CP moves to lower temperatures and finally disappears from the phase diagram. (See also Ref. [11] for a detailed discussion of this effect.)

Finally, we would like to comment on the slopes of the three phase transition lines in the LP. For $G_V = 0$ all of them are equal, i.e., the phase boundaries are tangential in the LP. In the $\tilde{\mu} - T$ plane, this remains of course true for $G_V > 0$. However, when we employ Eq. (15) to map $\tilde{\mu}$ onto μ we have to keep in mind that the average density $\bar{n}$ at given T and $\tilde{\mu}$ depends on the constituent quark mass M. The latter vanishes identically at the two phase boundaries to the restored phase, but is nonzero at the boundary between the homogeneous broken and the inhomogeneous phase, approaching zero only towards the LP. Depending on the corresponding critical exponent, this can affect the slope of this boundary in such a way that it meets the two others with a nonvanishing angle at $G_V > 0$. As one can see in Fig. 1, this is indeed the case.

2. Density profiles

The results presented above are based on the assumption that in the thermodynamic potential the density $n(\mathbf{x})$ can be approximated by its spatial average $\bar{n}$, see Eq. (8). Of course this approximation might appear questionable in an inhomogeneous phase. In order to get some insight into this issue, we now want to discuss the density profile $n(z)$ of the solitons. To that end we restrict ourselves to the case $G_V = 0$, where Eq. (8) does not enter into the derivation. To the extent that Eq. (8) is a good approximation, the results can then be translated to $G_V > 0$ by the mapping Eq. (15). For simplicity, we will also limit ourselves to the chiral limit, although this is not essential.

In mean-field the density profile is given by the expectation value

$$\begin{aligned} n(\mathbf{x}) &= \langle \psi^\dagger(\mathbf{x})\psi(\mathbf{x})\rangle \\ &= \frac{1}{2V}\sum_{E_i} \psi^\dagger_{E_i}(\mathbf{x})\psi_{E_i}(\mathbf{x})\left(n_+(E_i)-n_-(E_i)\right) , \end{aligned} \tag{23}$$

where the $\psi_{E_i}(\mathbf{x})$ are eigenfunctions of the Hamiltonian H_0 (see Eq. (5)) for the eigenvalues E_i and $n_\pm(E)$ are the Fermi occupation numbers defined below Eq. (16).
For one-dimensional modulations the energy spectrum is highly degenerate and we can label the eigenvalues as $E=\sqrt{\lambda^2+\mathbf{p}_\perp^2}$, where $\mathbf{p}_\perp$ is the conserved momentum of the quasi-particle perpendicular to the modulation and λ is the eigenvalue of the Hamiltonian at $\mathbf{p}_\perp=0$. The latter reduces to the Gross-Neveau Hamiltonian and we refer to Ref. [43] for details. Since $\psi^\dagger_E(z)\psi_E(z)$ in this case only depends on λ, we arrive at

$$n(z) = \frac{2N_c}{V}\int d\lambda\,\rho_1(\lambda)\int\frac{dp_\perp}{(2\pi)^{d_\perp}}\psi^\dagger_\lambda(z)\psi_\lambda(z)\left(n_+(E)-n_-(E)\right) , \tag{24}$$

where $\rho_1(\lambda)$ is the spectral density of the one-dimensional GN model [36–39] and

$$\psi^\dagger_\lambda(z)\psi_\lambda(z) = \frac{(\lambda/\Delta)^2+\frac{1}{2}((M(z)/\Delta)^2+\nu-2)}{(\lambda/\Delta)^2-\mathbf{E}(\nu)/\mathbf{K}(\nu)} . \tag{25}$$

Similar to the determination of the effective density of states, Eq. (18) (see Ref. [43] for details), it is then a tedious, but straightforward exercise to cast the expression for the density profile into the form

$$n_{\rm soliton}(z) = 2N_c\int_0^\infty dE\,\rho_{D,{\rm soliton}}(E,z)\left(n_+(E)-n_-(E)\right) , \tag{26}$$

where the density matrix element $\rho_{D,{\rm soliton}}(E,z)$ can be related to $\rho_{\rm soliton}(E)$, Eq. (18), upon the replacement

$$\rho_{D,{\rm soliton}}(E,z) = \rho_{\rm soliton}(E)\Big|_{\frac{\mathbf{E}(\nu)}{\mathbf{K}(\nu)}\to-\frac{1}{2}\left(\left(\frac{M(z)}{\Delta}\right)^2+\nu-2\right)} . \tag{27}$$

The resulting density profiles at $T=0$ and four different chemical potentials are shown in the lower part of Fig. 3. Comparing them with the corresponding mass functions $M(z)$, which are displayed in the upper part of the figure, we find that the density distributions follow closely the positions of the solitons, i.e., of the zero-crossings of the mass functions. In a bag-model like picture, this can be interpreted as the quarks being squeezed by the bag pressure of the domains with broken chiral symmetry into the regions of space where chiral symmetry is almost restored. From a topological point of view, these quarks are related to zero energy modes localized on the domain-wall.
These features are seen most clearly at $\mu=307.5$ MeV, which is just above the phase boundary from the homogeneous broken phase. Here the solitons are well separated, leading to strongly localized density peaks as functions of z. In this regime the assuption of a homogeneous density in order to obtain the solutions for $G_V>0$ is certainly poor. However, when μ is increased the solitons quickly start to overlap and the density profiles become more and more washed out. At

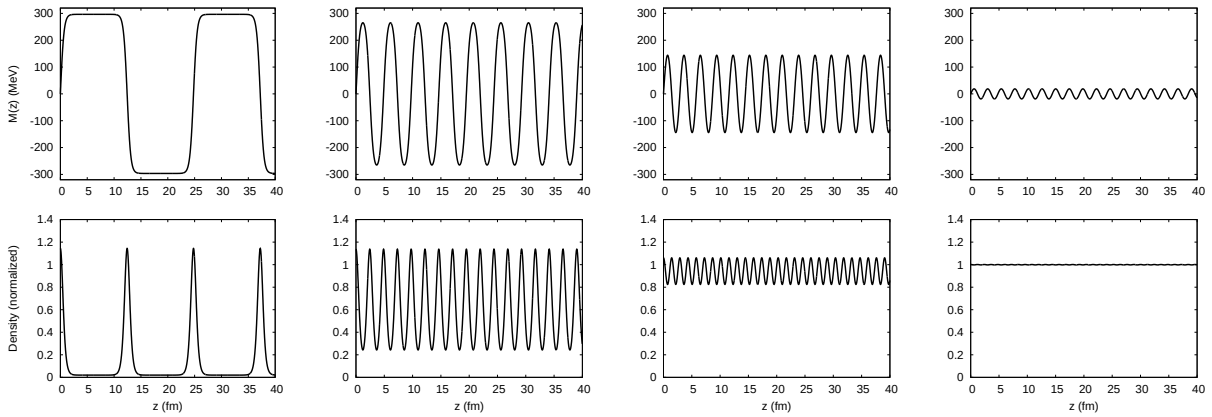

FIG. 3: Spatially dependent constituent mass function $M(z)$ (upper row) and corresponding density profile (lower row) at $G_V = 0$ and $m = 0$ for $T = 0$ and, from left to right, $\mu = 307.5$, 309, 325, and 345 MeV. The density is normalized to the density in the restored phase, $n_{rest} = \frac{2N_c}{3\pi^2}\mu^3$.

the second-order transition to the restored phase, the order parameter melts and the density profile smoothly approaches the uniform density of the restored phase. This is illustrated by the example of $\mu = 345$ MeV, which is close to the phase boundary. Note, however, that already at $\mu = 325$ MeV the density variations are relatively small.

The $T = 0$ results shown in Fig. 3 are the most extreme cases. With increasing temperature the mass functions melt and the density profiles become washed out by thermal effects. The assumption of a uniform density profile is therefore most questionable at the transition from the homogeneous broken to the inhomogeneous phase at low temperatures. In fact, at $G_V > 0$, a local density approximation would result in a lower value of $\tilde{\mu}$ within the solitons. This reflects the repulsive nature of the vector interaction, which disfavors localized density peaks. We therefore expect that the formation of well separated solitons, as we find near the boundary to the homogeneous broken phase at $T = 0$, eventually becomes inhibited by the vector interaction. Related to this, the second-order phase transition from the homogeneous broken to the inhomogeneous phase may partially turn into a first-order transition at $G_V > 0$.

On the other hand our assumption of a uniform density becomes gradually better with increasing μ or T and is fully justified at the phase transition line to the restored phase. In particular the phase boundary itself and the Lifshitz point are not affected by the approximation. This will be shown more rigorously in Sec. II D by a Ginzburg-Landau analysis.

3. Chiral density wave

Complementary support for the results of Sec. II C 1 can be obtained from investigations of the chiral spiral, Eq. (21). Although, at least at $G_V = 0$, this kind of modulation is disfavored compared to the domain-wall soliton [43], a constant density profile is no assumption here, but a property of the state. We can therefore perform a completely self-consistent mean-field calculation, leading

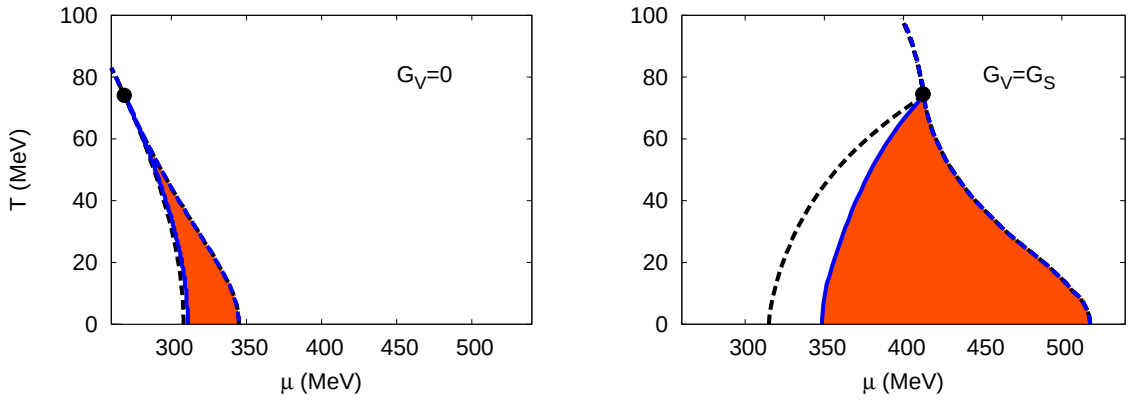

FIG. 4: Phase diagrams in the $\mu - T$ plane at $G_V = 0$ (left) and $G_V = G_S$ (right). The dashed lines have the same meaning as in Fig. 1 and represent the second-order phase boundaries between the homogeneous broken phase, the restored phase and the inhomogeneous phase with domain-wall solitons, respectively. The shaded area indicates the region where the CDW is favored compared to homogeneous phases (but not to the solitons). Here the blue solid line represents the first-order phase boundary from the broken homogeneous phase to the CDW, while the phase boundary from the CDW to the restored phase is second order and coincides with the boundary from the soliton phase to the restored phase.

to the phase diagrams shown in Fig. 4. The calculations have again been performed in the chiral limit and for $G_V = 0$ (left panel) and $G_V = G_S$ (right panel). The regions where the CDW is favored against the homogeneous broken and restored phases are indicated by the shaded areas. For comparison we have also indicated the boundaries of the regime where the solitons are favored (dashed lines).

As discussed in section II D below, the transition from the chiral spiral to the chirally restored phase is second order and agrees exactly with the transition from the soliton lattice to the restored phase. In particular, this also holds for the Lifshitz point. On the other hand, the transition from the homogeneous broken phase to the state where the chiral spiral is preferred is first order. For this reason, given the arguments of Sec. II C 1, it is directly depending on G_V, not only through $\tilde{\mu}$. As a result, the phase boundary, which at $G_V = 0$ almost coincides with the corresponding phase boundary of the soliton phase, moves away from it at $G_V = G_S$. However, this effect is rather mild. Moreover we find that the first-order transition line from the homogeneous broken phase to the chiral spiral is much less affected by the vector interaction than the second-order transition line from the chiral spiral to the restored phase. The qualitative behavior of the phase diagram as a function of G_V is therefore similar to our results for the soliton lattice. Since we expect the CDW to be disfavored compared to the solitons, we can take the CDW result as a lower limit for the area occupied by an inhomogeneous phase. This suggests that the effect of assuming a uniform density profile for the solitons is not drastic.

4. susceptibilites

The divergence of susceptibilities near a critical point has led to suggestions for how to locate the CP in the QCD phase diagram experimentally [45] and therefore attracted significant interest also in model studies. Since the CP as a cornerstone of the phase diagram is essentially replaced by the LP in our study, we first want to discuss the behavior in its vicinity. For simplicity we will limit ourselves to the number susceptibility

$$\chi_{nn} \quad = \quad -\frac{\partial^2 \Omega}{\partial \mu^2} \quad = \quad \frac{\partial \bar{n}}{\partial \mu}\,, \tag{28}$$

which corresponds to the change in density when going along a line of constant temperature. For this reason the behavior of χ_{nn} near the LP is in fact determined by the behavior when going from the homogeneous broken to the restored phase and not by the inhomogeneous phase. Consequently, since the LP coincides with the CP for $G_V = 0$, we find the same divergent behavior as when limiting to homogenous phases for $G_V = 0$. For completeness, this is illustrated on the right hand side of Fig. 5, showing a $1/\sqrt{\mu_{\rm cr} - \mu}$-like singulartity when approaching the LP from the left. However, for $G_V > 0$ the behavior is qualitatively altered: The would-be CP when limiting to homogeneous phases is hidden inside the domain of a inhomogeneous phase and the LP does not correspond to the endpoint of the second-order phase transition line when limiting to homogeneous phases. For this reason the number susceptibility does not diverge near the LP for $G_V > 0$. This can easily be understood in the context of a Ginzburg-Landau expansion as introduced in subsection II D and is related to the fact that $c_{4,a} \neq 0$ for $G_V > 0$ at the LP.

Focusing on $G_V = 0$ first and investigating the number susceptibility numerically in the regime where soliton lattices are energetically preferred, we find the results shown in Figs. 5, 6. Since all transition are second order, the averaged number density changes continuously when varying temperature and chemical potential. At the transition from the homogeneous broken to the inhomogeneous phase the change is however very rapid as discussed in the following and χ_{nn} diverges. This is most prominent at $T = 0$ and decreases when going towards the LP.

In order to get an intuition for the qualitative behavior of χ_{nn} we consider the GN model and focus on the density as a function of chemical potential $n_{GN}(\mu)$ at vanishing temperatures. As can be extracted from Refs. [36, 38] it is given by

$$n_{GN} \;=\; \frac{\pi^2}{2\nu \mathbf{K}(\nu)} M_0\,, \tag{29}$$

where M_0 as the fermion mass in the vacuum sets the scale and the elliptic modulus as a function of chemical potential is given through the implicit relation $\pi\sqrt{\nu}\mu = 2\mathbf{E}(\nu)M_0$. At the transition from homogeneous to inhomogeneous phase at $\mu_{cr} = \frac{2}{\pi}M_0$ the number density then behaves like

$$n_{GN} \;\simeq\; -\frac{\pi^2 M_0}{\ln(\mu/\mu_{cr} - 1)}\,, \tag{30}$$

which leads to a $[(\mu - \mu_{cr})\log^2(\mu - \mu_{cr})]^{-1}$-like singularity in the number susceptibility.

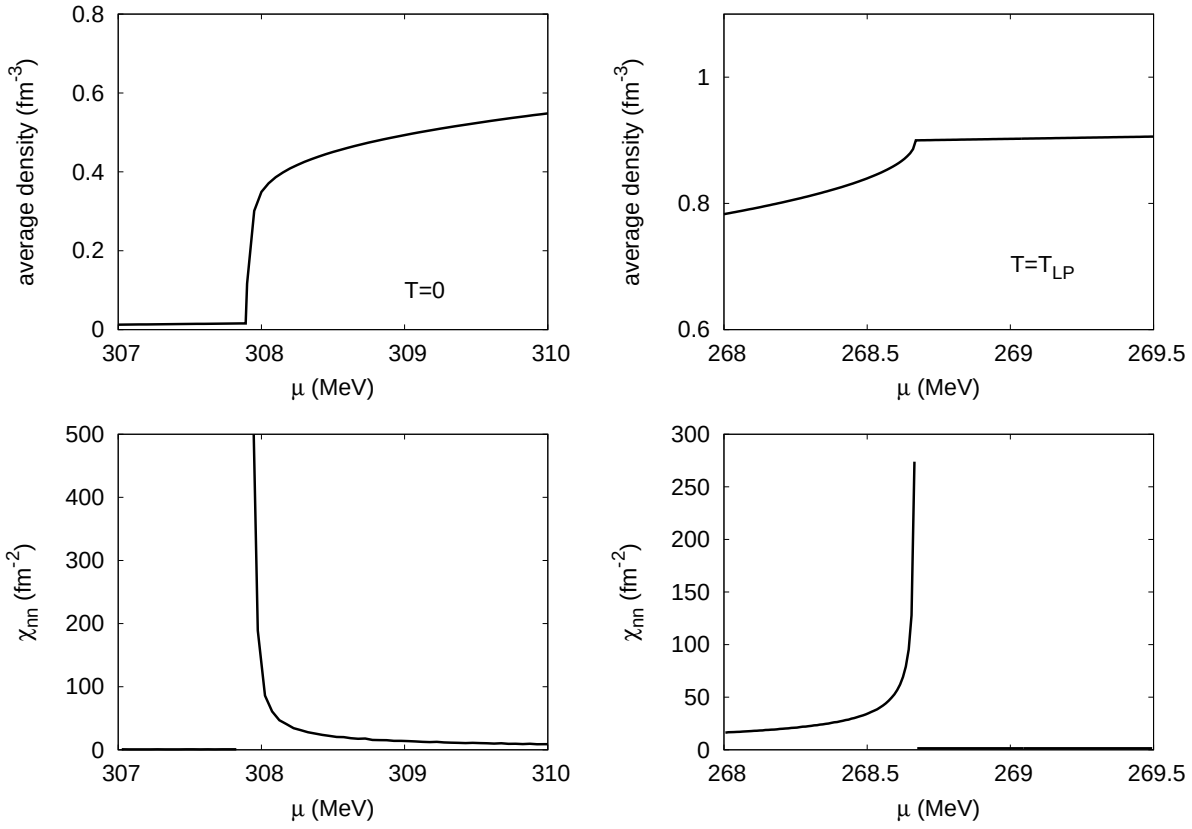

FIG. 5: Averaged density (upper panel) and number susceptibility (lower panel) for vanishing temperatures (left) and for the temperature at the LP (right) as a function of chemical potential and for $G_V = 0$.

A straightforward generalization of Eq. (30) to three spatial dimensions suggests that for $G_V = 0$ the change $\Delta\bar{n}$ in the average number density near the transition from the broken homogeneous to the inhomogeneous phase at $\mu = \mu_{cr}(T)$ should be given by

$$\Delta\bar{n} \;=\; -\frac{c\mu_{cr}^3}{\ln(\mu/\mu_{cr} - 1)}\,, \tag{31}$$

with some temperature-dependent coefficient c. Indeed, our numerical results are consistent with this behavior, thus explaining the divergence of χ_{nn} at $\mu = \mu_{cr}$.
In contrast, for $G_V > 0$ the mapping $\tilde{\mu} \to \mu$ via Eq.(15) leads to a qualitatively different behavior. For this case we find

$$\chi_{nn} \quad = \quad \frac{\partial n}{\partial\tilde{\mu}} \Big/ \frac{\partial\mu}{\partial\tilde{\mu}} \quad = \quad \frac{1}{1 + 2G_V \frac{\partial n}{\partial\tilde{\mu}}} \frac{\partial n}{\partial\tilde{\mu}}\bigg|_{\tilde{\mu}(\mu)} \,. \tag{32}$$

Therefore a divergence in $\partial n/\partial\mu$ at $G_V = 0$ does not result in a divergent number susceptibility for $G_V > 0$, but merely leads to a jump of order $1/2G_V$. This is illustrated on the right hand side of Fig. 6.

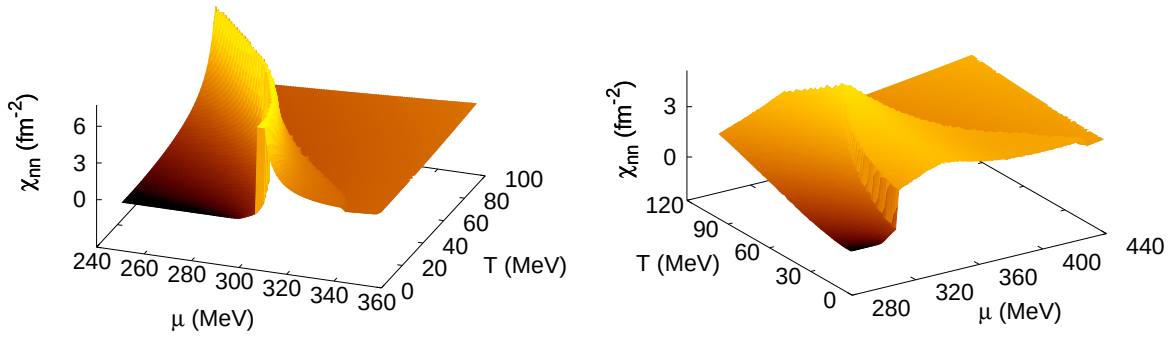

FIG. 6: Number susceptibility in the $\mu - T$ plane at $G_V = 0$ (left) and $G_V = G_S/2$ (right). For $G_V = 0$ the number susceptibility diverges at the transition from broken to inhomogeneous phase.

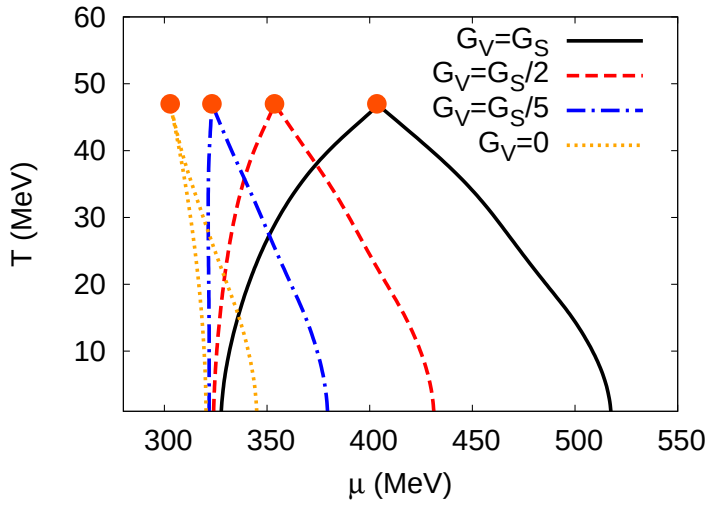

FIG. 7: $\mu - T$ phase diagram for different values of G_V and a current quark mass $m = 5\,\mathrm{MeV}$. The dots indicate the Lifshitz points above which the second order transition lines join and turn into a crossover.

5. *Finite current quark masses*

For completeness we present in Fig. 7 our results for the phase diagram at a non-vanishing current quark mass $m = 5$ MeV and various values of G_V by considering Eq. (19). Since there is no exact order parameter to distinguish the homogeneous broken from the restored phase in this case, there are strictly speaking only two phases – a homogeneous and an inhomogeneous phase – and, hence, no Lifshitz point. Nevertheless we can easily identify the remnant of the LP as a cusp in the phase boundary. For simplicity, we will call this point a Lifshitz point as well.

It has already been observed [43] that the LP shifts to smaller temperatures and larger chemical potentials when increasing m. The dependence on G_V however stays qualitatively the same as in the chiral limit: the LP is only shifted in the μ-direction upon increasing G_V and the domain

of inhomogeneous phases in the $\mu - T$ diagram is stretched. The explanation for this behavior is identical to the one given in section II C 1 for the chiral limit.

D. Ginzburg-Landau expansion

In the vicinity of a second-order phase transition and in particular of a critical point, the thermodynamic potential can be studied systematically within a Ginzburg-Landau expansion. In the present case, this corresponds to an expansion of the thermodynamic potential as an effective action in $\delta M(\mathbf{x}) = M(\mathbf{x}) - M_0$ and $\delta\tilde{\mu}(\mathbf{x}) = \tilde{\mu}(\mathbf{x}) - \tilde{\mu}_0$ around their values $M(\mathbf{x}) = M_0$ and $\delta\tilde{\mu}(\mathbf{x}) = \tilde{\mu}_0$ in the restored phase. For simplicity, we restrict ourselves to the chiral limit, so that $M_0 = 0$ and therefore $\delta M(\mathbf{x}) = M(\mathbf{x})$. However, unlike in the numerical studies above, we will not assume $\tilde{\mu}(\mathbf{x})$ to be spatially uniform.

At given temperature and chemical potential the expansion then takes the form

$$\Omega[M, \tilde{\mu}] \;=\; \Omega[0, \tilde{\mu}_0] + \frac{1}{V}\int d\mathbf{x}\, \Omega_{GL}(M(\mathbf{x}), \delta\tilde{\mu}(\mathbf{x}))\,, \tag{33}$$

with

$$\begin{aligned}
&\Omega_{GL}(M(\mathbf{x}), \delta\tilde{\mu}(\mathbf{x})) \\
&= \; c_{2,a}|M(\mathbf{x})|^2 + c_{2,b}\delta\tilde{\mu}(\mathbf{x})^2 + c_{3,a}|M(\mathbf{x})|^2\delta\tilde{\mu}(\mathbf{x}) + c_{3,b}\delta\tilde{\mu}(\mathbf{x})^3 \\
&\quad + c_{4,a}|M(\mathbf{x})|^4 + c_{4,b}|\nabla M(\mathbf{x})|^2 + c_{4,c}|M(\mathbf{x})|^2\delta\tilde{\mu}(\mathbf{x})^2 + c_{4,d}\delta\tilde{\mu}(\mathbf{x})^4 + c_{4,e}(\nabla\delta\tilde{\mu}(\mathbf{x}))^2 + \dots\,,
\end{aligned} \tag{34}$$

when expanding to fourth order in $M(\mathbf{x})$, $\delta\tilde{\mu}(\mathbf{x})$ and gradients acting on these functions. The symmetries of the theory and of the background simplify the expansion: linear terms vanish as we are expanding around a homogeneous solution of the gap equations, odd terms in $M(\mathbf{x})$ vanish by chiral symmetry and odd numbers of derivatives vanish due to rotational symmetry.

Taking $M(\mathbf{x})$ to be the small scale of interest, we first aim at an estimate for $\delta\tilde{\mu}(\mathbf{x}; M(\mathbf{x}))$ defined through the stationary constraint

$$\left.\frac{\delta\Omega}{\delta\delta\tilde{\mu}}\right|_{M(\mathbf{x}),\delta\tilde{\mu}(\mathbf{x})=\delta\tilde{\mu}(\mathbf{x};M(\mathbf{x}))} \;=\; 0\,. \tag{35}$$

Because of the absence of a linear term in $M(\mathbf{x})$ we conclude that $\delta\tilde{\mu}(\mathbf{x}; M(\mathbf{x})) \sim O(|M(\mathbf{x})|^2)$. More precisely,

$$\delta\tilde{\mu}(\mathbf{x}; M(\mathbf{x})) = -\frac{c_{3,a}}{2c_{2,b}}|M(\mathbf{x})|^2 + \dots\,. \tag{36}$$

Consequently, the expansion of $\Omega_{GL}(M(\mathbf{x})) \equiv \Omega_{GL}(M(\mathbf{x}), \delta\tilde{\mu}(\mathbf{x}; M(\mathbf{x})))$ to fourth order is given by

$$\Omega_{GL}(M(\mathbf{x})) \;=\; \Omega_{GL}[0, \tilde{\mu}_0] + c_{2,a}|M(\mathbf{x})|^2 + \left(c_{4,a} - \frac{c_{3,a}^2}{4c_{2,b}}\right)|M(\mathbf{x})|^4 + c_{4,b}|\nabla M(\mathbf{x})|^2 + \dots\,, \tag{37}$$

which allows us to determine the Lifshitz and the critical points from the GL coefficients. The latter is characterized by vanishing quadratic and quartic mass terms, while at the former the

quadratic term and the gradient term are zero:

$$\begin{aligned} \text{LP:} \quad & 0 = c_{2,a} = c_{4,b}\,, \\ \text{CP:} \quad & 0 = c_{2,a} = c_{4,a} - \frac{c_{3,a}^2}{4c_{2,b}}\,. \end{aligned} \tag{38}$$

As outlined in Ref. [44] for the NJL model without vector interactions, it is a straightforward exercise to work out the explicit form of the GL coefficients. As obvious from Eqs. (4) and (5), the kinetic part of the thermodynamic potential, Ω_{kinetic}, and, hence, its contributions to the GL coefficients depend on G_V only indirectly through $\tilde{\mu}_0$ and T. The only explicit dependence on G_V therefore originates from Ω_{cond} and only affects $c_{2,b}$. For this reason the Lifshitz point as a function of $\tilde{\mu}_0$ and T is independent of G_V, in agreement with our findings in section II C.

In contrast there is an explicit dependence of the location of the critical point on G_V through $c_{2,b}$. One finds

$$c_{2,b} = -\frac{1}{4G_V} - N_c \left(\frac{\tilde{\mu}_0^2}{\pi^2} + \frac{T^2}{3} \right)\,, \tag{39}$$

where the first term on the right hand side is due to Ω_{cond}, while the second term is due to Ω_{kinetic}. Since we are expanding around a homogeneous restored solution, the latter is just given by the corresponding term in an ideal Fermi gas at temperature T and chemical potential $\tilde{\mu}_0$. Here we have neglected the contributions from the regulator terms, which would arise in our specific model. However, these terms are small in the region of interest and therefore do not lead to qualitative changes. Hence, $1/c_{2,b}$ vanishes for $G_V = 0$ and decreases monotonously with increasing positive values of G_V. Furthermore $c_{4,a}$ typically decreases when increasing $\tilde{\mu}_0$ or decreasing T in the vicinity of the critical point. Put together, we conclude from Eq. (38) that the CP moves to smaller temperatures upon increasing G_V. Moreover, discarding possible issues related to the regularization of the UV-divergent vacuum contribution to the thermodynamic potential[2], we find $c_{4,a} = c_{4,b}$, as in the case without vector interaction [44]. For $G_V = 0$ we therefore recover the result of Ref. [44] that the LP and the CP coincide.

Since $\delta\tilde{\mu}(\mathbf{x}) \sim O(M(\mathbf{x})^2)$ we can also conclude that the thermodynamic potential expanded around $\tilde{\mu}_0$ to order $O(|M(\mathbf{x})|^2)$ and arbitrary gradients coincides with that of the model for $G_V = 0$ upon replacing $\mu \to \tilde{\mu}_0$. As a result, the second-order phase transition from any inhomogeneous to the chirally restored phase, being triggered by these contributions, is only depending on G_V through $\tilde{\mu}_0$, as it was already obtained in section II C by applying further truncations.

On the other hand, the present analysis is not applicable to the transition from the homogeneous broken to inhomogeneous phase, where the mass function is not related to a small parameter, when we go away from the LP. As we have argued earlier, even the order of the phase transition may change in this regime when vector interactions are included.

Qualitatively the same properties as discussed here for the NJL model with a vector interaction also show up in the Gross-Neveu model with a Thirring interaction (GNT model) at leading order

[2] For a renormalizable theory divergent GL coefficients are subject to renormalization; the present discussion is consistent for a regularization scheme acting on the energy spectrum as applied in this work.

in the large N-expansion. Since the model is renormalizable and therefore much cleaner and easier to handle, we include a discussion of its phase diagram in Appendix A.

III. EFFECTS OF POLYAKOV LOOP DYNAMICS

A. Inclusion of the Polyakov loop

In order to mimic features of confinement, in particular to suppress the contribution of free constituent quarks in the confined phase, and in order to include gluonic contributions to the pressure, the NJL model can be coupled to an effective description of the Polyakov loop [13, 14]. The resulting model is known as the Polyakov-loop extended Nambu–Jona-lasinio (PNJL) model.
The Polyakov loop is defined by

$$L(\mathbf{x}) = \mathcal{P} \exp\left[i \int_0^{1/T} d\tau \, A_4(\tau, \mathbf{x}) \right] , \tag{40}$$

where $A_4(\tau, \mathbf{x}) = iA_0(t = -i\tau, \mathbf{x})$ is the temporal part of a gauge field $A_\mu = g A_\mu^a \frac{\lambda^a}{2}$ at imaginary time. In pure Yang-Mills theory, the traced expectation values of L and its hermitean conjugate,

$$\ell = \frac{1}{N_c} \langle \mathrm{Tr}_c L \rangle \, , \qquad \bar{\ell} = \frac{1}{N_c} \langle \mathrm{Tr}_c L^\dagger \rangle \, , \tag{41}$$

can be related to the free energies of a static quark or antiquark, $\ell \sim e^{-F_q/T}$, $\bar{\ell} \sim e^{-F_{\bar{q}}/T}$ [50, 51], and are therefore order parameters for the confinement-deconfinement transition.
To include the Polyakov-loop dynamics in the NJL model, the quarks are minimally coupled to a background gauge field, $\partial_\mu \to D_\mu = \partial_\mu + iA_0\delta_{\mu 0}$. Furthermore, a local potential $\mathcal{U}(\ell, \bar{\ell})$ is added to the thermodynamic potential, which is essentially constructed to reproduce ab-initio results of pure Yang-Mills theory at finite temperature [14, 52]. In the most simple approach, the gauge field is taken to be a space-time independent mean field A_4, and the effect of the covariant derivative in the kinetic part amounts to the replacement [13]

$$\begin{aligned} f_{\mathrm{thermal}}(E) \;\to\; f_{\mathrm{thermal,PNJL}}(E) &= T \ln\left(1 + \mathrm{e}^{-3(E-\mu)/T} + 3\,\ell\,\mathrm{e}^{-(E-\mu)/T} + 3\,\bar{\ell}\,\mathrm{e}^{-2(E-\mu)/T} \right) \\ &\quad + T \ln\left(1 + \mathrm{e}^{-3(E+\mu)/T} + 3\,\bar{\ell}\,\mathrm{e}^{-(E+\mu)/T} + 3\,\ell\,\mathrm{e}^{-2(E+\mu)/T} \right) . \end{aligned} \tag{42}$$

However, as can be seen from Eqs. (40) and (41), a constant mean field A_4 would always result in complex conjugate values for ℓ and $\bar{\ell}$. This should be considered as an artifact, since their interpretation as being related to the free energies of quarks and antiquarks means that ℓ and $\bar{\ell}$ should be real and, at finite chemical potential, different from each other. In order to by-pass this problem, we therefore follow the viewpoint of Ref. [10] that, after the replacement (42), ℓ and $\bar{\ell}$ should be treated as independent real mean fields, rather than the components of A_4. This is also consistent with the fact that the potential $\mathcal{U}$ which is added to the thermodynamic potential is given in terms of ℓ and $\bar{\ell}$ as well. For simplicity we take Fukushima's parametrization [10],

$$\mathcal{U}(\ell, \bar{\ell}) \;=\; -b\,T \left(54\,\mathrm{e}^{-a/T}\,\ell\,\bar{\ell} + \log\left[1 - 6\,\ell\,\bar{\ell} - 3(\ell\,\bar{\ell})^2 + 4(\ell^3 + \bar{\ell}^3) \right] \right) \tag{43}$$

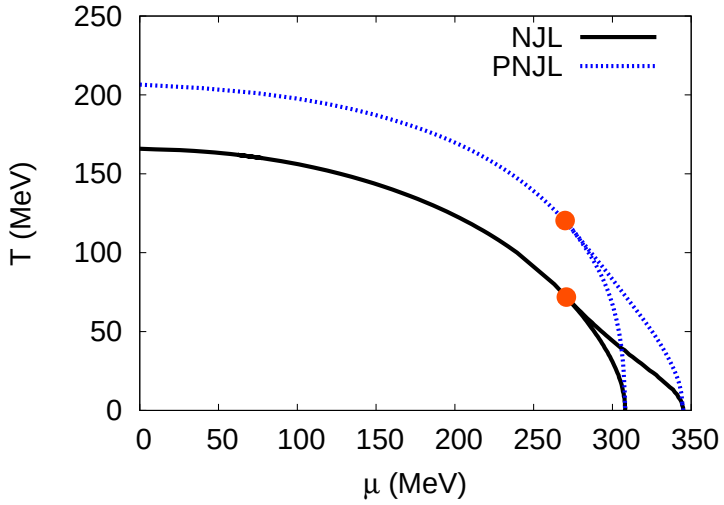

FIG. 8: Phase diagram of the NJL (solid line) and PNJL (dashed line) model allowing for one-dimensional spatial modulations of the order parameter.

with two parameters a and b. Other prescriptions, like the polynomial [14] or the logarithmic [52] potential, would lead to very similar results.

When dealing with inhomogeneous phases, ℓ and $\bar{\ell}$ are naturally expected to be spatially dependent, presumably following the density profile in some way. Nevertheless, similar to the treatment of $\tilde{\mu}$ in the previous section, we will assume spatially independent values of ℓ and $\bar{\ell}$, even in the inhomogeneous phase. This is not only to keep the technical side of the calculation trackable, but also the assumptions made in order to derive (42) and the unknown kinetic contributions to Eq. (43) suggest such a conservative approach as a first step.

To summarize, we obtain a thermodynamic potential

$$\Omega_{\mathrm{PNJL}} \;=\; \Omega_{\mathrm{kinetic}}|_{f_{\mathrm{thermal}}\to f_{\mathrm{thermal,PNJL}}} + \Omega_{\mathrm{cond}} + \mathcal{U}(\ell,\bar{\ell})\,, \tag{44}$$

with $\Omega_{\mathrm{kinetic}}$ and Ω_{cond} given in Eqs. (4)-(11), that additionally needs to be extremized in ℓ and $\bar{\ell}$.

B. Numerical results

Since we consider the NJL model with $G_V = m = 0$ as our starting point, we shall limit ourselves to this case when studying the role of the Polyakov loop. For the Polyakov-loop potential, we adopt the parameters of Ref. [10], $a = 664\,\mathrm{MeV}$ and $b = 7.55 \cdot 10^6\,\mathrm{MeV}^3$. The parameter a was fixed by the condition that for pure gluo-dynamics the phase transition takes place at $T = 270$ MeV, while b was chosen to have a crossover around $T = 200$ MeV at $\mu = 0$ when quarks are included. Since we are mainly interested in the qualitative effect of the Polyakov loop, we did not perform a refit of b within our regularization scheme. We checked, however, that this parameter choice gives reasonable results for the behavior of the order parameters at $\mu = 0$.

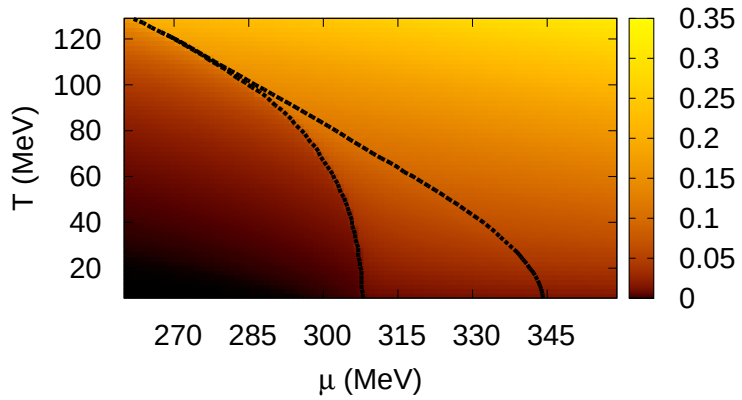

FIG. 9: Polyakov loop expectation value ℓ in the μ-T plane in the vicinity of the inhomogeneous phase.

In Fig. 8 we compare the phase diagrams for the NJL model with that of the PNJL model, allowing for phases with a one-dimensional solitonic modulation in both cases. Aside from a general stretching in the T-direction, which is well known from studies of homogeneous phases and easily explained by the replacement (42), the Polyakov loop has no effect on the qualitative structure of the phase diagram. In particular, the critical point at $G_V = 0$ still coincides with the Lifshitz point.

In Fig. 9 the value of ℓ is presented via color coding in the region of the phase diagram where the inhomogeneous phase is favored. We find that ℓ and $\bar{\ell}$ are rather small in the entire inhomogeneous phase, reaching their maximum values $\ell \approx 0.15$ and $\bar{\ell} \approx 0.2$ near the LP. In this context we should recall that at vanishing temperature the Polyakov-loop dynamics decouples completely from the quark sector due to the way the PNJL model is constructed. As a consequence, $\ell = \bar{\ell} = 0$ at $T = 0$, independent of the density. While it is unclear whether this feature of the model is realistic, it means that our assumption of space-independent Polyakov-loop expectation values cannot have a large effect. Even if ℓ and $\bar{\ell}$ followed the density profile, the results would not be very different, because at low temperatures their values are very small anyway, whereas at higher temperatures the density differences get washed out.

IV. DISCUSSION

In this work we have analyzed the role of the isoscalar-vector interaction and the dynamics of the Polyakov loop on recently discussed inhomogeneous ground states in the phase diagram of the NJL model. Mainly for technical reasons we thereby limited ourselves to inhomogeneous phases with a one-dimensional modulation, explicitly to domain-wall soliton lattices and for comparison to chiral spirals. This allowed us to exploit the knowledge obtained for lower dimensional models in our study.

Our previous study in absence of vector interactions has led us to the finding that the critical point in the mean-field phase diagram of the NJL model actually coincides with a Lifshitz point when allowing for the possibility of inhomogeneous phases. The first order phase transition is then absent in the phase diagram, since an inhomogeneous phase is energetically preferred in its domain. When extending our model, we find that a repulsive vector interaction leads to significant qualitative effects: In contrast to the critical point when limiting to homogeneous phases, the Lifshitz point is not shifted towards smaller temperatures when increasing the strength of the vector interaction, but remains at the same temperature and density. Moreover, the domain of inhomogeneous ground states in the $\mu - T$ phase diagram increases. Since the Lifshitz point therefore no longer coincides with the critical point, the critical behavior in its vicinity and also near the phase transition lines to the inhomogeneous phase changes. This is underlined by the fact that the number susceptibilities remain finite, i.e., there are no singularities.

Our investigation of this part is complemented by an extensive numerical study, including the determination of density profiles in the inhomogeneous phase, the phase diagram when only allowing for chiral spirals, the evaluation of number susceptibilities and the incorporation of finite current quark masses. Furthermore, we performed a generalized Ginzburg-Landau expansion for elaborating the dependence of Lifshitz and critical point on the vector interaction and we mapped out the phase diagram of the $1+1$-dimensional GN model with a Thirring interaction. Part of this comprehensive study is also motivated in order to back up an approximation employed within our mean-field calculation, namely to use the spatially averaged number density when evaluating the thermodynamic potential.

Probably less spectacular but nevertheless worth checking is the behavior of our model when the quarks are coupled to the Polyakov loop in order to suppress their contribution to the thermodynamic potential in chirally broken phases, thus mimicking confinement. In the absence of a vector interaction this coupling, at least in the employed approximation, does not lead to a separation of Lifshitz and critical point. Consequently the $\mu - T$ phase diagram is not modified qualitatively and, similar as in the case of homogeneous phases, is only stretched in the temperature direction.

Our analysis has shown that the region where solitonic modulations of the chiral order parameter are favored over homogeneous phases increases when considering natural extensions of the two-flavor NJL model. Although being much more tractable on the technical side, it is worth noting that strictly speaking one-dimensional modulations of the order parameter are washed out by thermal fluctuations at finite temperature [53, 54]. This statement refers to the fact that the modulation is not rigid, but fluctuates locally. The system's spatially modulated nature is however still encoded in the behavior of long range correlations. To get past this kind of issue, it would anyway be of great interest to extend the present analysis to inhomogeneous phases with higher dimensional modulations. This should be possible in a more numerical approach as outlined in Ref. [31] in the context of inhomogeneous color-superconducting phases. The most interesting question here is whether the transition from the inhomogeneous to the restored phase can turn first order for more complex modulations at low enough temperatures. E.g. for color-superconducting phases, this has been suggested in Ref. [27], although the applied expansion did not allow for a conclusive answer.

Acknowledgments

The authors would like to thank B. Friman, K. Fukushima, C. Tsallis, and J. Wambach for helpful comments and discussions. This work was partially supported by the Department of Energy (DOE) under grant numbers DE-FG02-00ER41132 and DE-FG0205ER41360, by the German Research Foundation (DFG) under grant number Ni 1191/1-1, by the Helmholtz research school for Quark Matter studies (H-QM), and by the Helmholtz Alliance EMMI.

Appendix A: The Gross-Neveu model with a Thirring interaction

To back up our results related to the vector interaction we briefly want to discuss its effect in the Gross-Neveu model with a Thirring interaction (GNT model). Unlike the NJL model, the GNT model is renormalizable and therefore does not suffer from regularization artifacts. The relevant Lagrangian is given by

$$\mathcal{L} \;=\; \bar{\psi}\left(i\gamma^\mu\partial_\mu - m\right)\psi + \frac{G_S}{2N}\left(\bar{\psi}\psi\right)^2 - \frac{G_V}{2N}\left(\bar{\psi}\gamma^\mu\psi\right)^2 , \tag{A1}$$

where ψ is a $2N$-dimensional spinor for N species in $1+1$ dimensions and γ^μ can be chosen as $\gamma^0=\sigma^1$, $\gamma^1=-i\sigma^2$, σ^i being the usual Pauli matrices.
In the large N-limit the mean-field approximation becomes exact.[3] Furthermore, since the model is renormalizable, all divergencies can be absorbed into a finite number of contact terms. The thermodynamic potential is given by

$$\begin{aligned}
\Omega_{\rm GNT}/N &= \Omega_{\rm kinetic}/N + \Omega_{\rm cond}/N\,,\\
\Omega_{\rm kinetic}/N &= -\frac{T}{L}\sum_n {\rm Tr}_{D,L}{\rm Log}\left(\frac{1}{T}(i\omega_n + F)\right)\,,\\
\Omega_{\rm cond}/N &= \frac{1}{L}\int dz\left(\frac{(M(z)-m)^2}{2G_S} - \frac{(\tilde{\mu}(z)-\mu)^2}{2G_V}\right)\,,
\end{aligned} \tag{A2}$$

where we introduced a similar notation as in the case of the NJL model: L is the periodicity, the spatial coordinate is labelled z, $M(z)=m-G_S\langle\bar{\psi}\psi\rangle/N$, $\tilde{\mu}(z)=\mu-G_V\langle\bar{\psi}\gamma^0\psi\rangle/N$ and

$$F \;=\; -i\gamma^0\gamma^1\partial_z + \gamma^0 M(z) - \tilde{\mu}(z)\,. \tag{A3}$$

For this setup we first investigate the phase diagram of homogeneous phases, in particular the role of G_V, and subsequently also inhomogeneous phases by means of a Ginzburg-Landau expansion. For homogeneous phases the eigenvalue spectrum of F can be labelled by the momenta and it is straightforward to obtain

$$\Omega_{\rm GNT}/N \;=\; \underbrace{-2\int_0^\Lambda \frac{dp}{2\pi}E_p + \frac{(M-m)^2}{2G_S} - \frac{(\tilde{\mu}-\mu)^2}{2G_V}}_{\equiv\Omega_{\rm vacuum}} \underbrace{-2T\int_0^\infty \frac{dp}{2\pi}\sum_{s=\pm}\ln\left(1+e^{-\frac{E_p+s\tilde{\mu}}{T}}\right)}_{\equiv\Omega_{\rm thermal}}, \tag{A4}$$

[3] Note that this limit does not commute with the thermodynamic limit.

where $E_p = \sqrt{p^2 + M^2}$. For $\Omega_{\rm vacuum}$ we introduced a sharp momentum cutoff Λ as the integral is divergent. Note, however, that for a renormalizable theory - in contrast to the NJL model - the regularization scheme is only introduced intermediately and does not affect the final results. We also note that the argument of the vacuum contribution should in principle contain the eigenvalues $\pm E_p - \tilde{\mu} + \mu$,[4] but for a sharp momentum cutoff this does not affect the renormalization procedure at large momenta. Concerning the ultraviolet behavior, we observe that the quadratic divergency can be absorbed into an order parameter independent constant, a linear and a quadratic term in M, corresponding to a renormalization of the overall pressure at $M = 0$, the fermion mass m and the coupling G_S. Requiring the thermodynamic potential to vanish at $M = \langle\bar{\psi}\gamma^0\psi\rangle = 0$ and to have a minimum at M_0, we then get

$$\Omega_{\rm vacuum}/N \;=\; \frac{1}{4\pi}M^2\left(-1 + 2\ln\frac{M}{M_0}\right) + \frac{cM\,(M-2M_0)}{2M_0} - \frac{(\tilde{\mu}-\mu)^2}{2G_V}\,, \tag{A5}$$

where c is proportional to m at finite Λ and not relevant here as we shall consider the chiral limit $c = 0$ in the following. G_V remains finite and can be assumed to have its renormalized value. In order to discuss the phase diagram all that is left is to extremize the potential in M and $\tilde{\mu}$. For simplicity we will focus the discussion on phase transitions and the location of the critical point. Addressing phase transitions between homogeneous phases, we first expand the thermodynamic potential in the constituent mass around $M = 0$. Similar to the GN model [55] we find

$$\Omega_{\rm GNT}/N \;=\; \sum_{n\geq 0}\alpha_{2n}(\tilde{\mu})M^{2n} \tag{A6}$$

with

$$\begin{aligned}
\alpha_0(\tilde{\mu}) \;&=\; -\frac{\pi T^2}{6} - \frac{\tilde{\mu}^2}{2\pi} - \frac{(\tilde{\mu}-\mu)^2}{2G_V}\,,\\
\alpha_2(\tilde{\mu}) \;&=\; \frac{1}{2\pi}\left(\ln\left(\frac{4\pi T}{M_0}\right) + \mathrm{Re}\,\psi(z)\right)\,,\\
\alpha_{2n}(\tilde{\mu}) \;&=\; -\frac{(-1)^n}{2^{2n-1}(n-1)(2n-4)!!(2n)!!\pi^{2n-1}T^{2n-2}}\mathrm{Re}\,\psi(2n-2,z)\,,\quad n>1\,,
\end{aligned} \tag{A7}$$

where we used the di- and polygamma functions and $z = \frac{1}{2} + \frac{i\tilde{\mu}}{2\pi T}$. Note that only α_2 is affected by the renormalization procedure. From the additional constraint $\partial\Omega_{\rm GNT}/\partial\tilde{\mu} = 0$ we can then infer the value $\tilde{\mu}_0 = \frac{\pi\mu}{\pi+G_V}$ of the renormalized chemical potential at $M = 0$ and furthermore expand in $\delta\tilde{\mu} = \tilde{\mu} - \tilde{\mu}_0$. For the purpose of our discussion, we can then limit ourselves to

$$\Omega_{\rm GNT}/N \;=\; \Omega_{\rm unbroken} + \alpha_{2,0}M^2 + \alpha_{4,0}M^4 + \alpha_{2,1}M^2\delta\tilde{\mu} + \alpha_{0,2}\delta\tilde{\mu}^2 + O(M^6, \delta\tilde{\mu}^3, M^2\delta\tilde{\mu}^2, M^4\delta\tilde{\mu})\,, \tag{A8}$$

[4] This is related to the fact that, like the constituent mass M, the density $\langle\bar{\psi}\gamma^0\psi\rangle \propto \mu - \tilde{\mu}$ is undetermined before the gap equations are solved.

where $\alpha_{n,0} = \alpha_n|_{\tilde{\mu}=\tilde{\mu}_0}$ and

$$\begin{aligned}\Omega_{\rm unbroken} \equiv \alpha_{0,0} &= -\frac{\pi T^2}{6} - \frac{\mu^2}{2(\pi + G_V)}\,,\\ \alpha_{2,1} &= -\frac{1}{4\pi^2 T}{\rm Im}\,\psi(1,z)|_{\tilde{\mu}=\tilde{\mu}_0}\,,\\ \alpha_{0,2} &= -\frac{\pi + G_V}{4\pi G_V}\,.\end{aligned} \tag{A9}$$

We conclude that $\delta\tilde{\mu} = -\frac{\alpha_{2,1}}{2\alpha_{0,2}}M^2 + O(M^3)$ and arrive at an expansion of the thermodynamic potential only depending on M,

$$\Omega_{\rm GNT}/N = \Omega_{\rm unbroken} + \alpha_{2,0}M^2 + \beta_4 M^4 + O(M^6)\,, \tag{A10}$$

where

$$\beta_4 = \alpha_{4,0} - \frac{\alpha_{2,1}^2}{4\alpha_{0,2}}\,. \tag{A11}$$

The critical point is then given by $\alpha_{2,0} = \beta_4 = 0$. As a simple exercise we can evaluate this condition at zero temperature, for which one finds $\ln(2\tilde{\mu}_0/M_0) = -1 + \frac{3}{\pi}G_V = 0$. At $G_V = \pi/3$ we have therefore a critical point at $T = 0$ and $\tilde{\mu} = 2M_0/3$. However, as illustrated in Fig.(10), it turns out that this is a "new" CP, which moves upwards in temperature upon increasing G_V. On the other hand, the "old" CP, existing already at $G_V = 0$, moves downwards, similar to the NJL model. Eventually, at $G_V \simeq 1.175$, both points merge and no first-order phase transition is left at higher values of G_V.

Turning to inhomogeneous phases, we can perform a generalized Ginzburg-Landau expansion. As in the NJL-model case, discussed in Sec. II D, this corresponds to an expansion of (A2) in $M(z)$ and $\delta\tilde{\mu}(z) = \tilde{\mu}(z) - \tilde{\mu}_0$, combined with a derivative expansion in order to obtain a local functional. The technology has been worked out in great detail for the GN model [38] and equally works for the GNT model. Since a $M(z)\delta\tilde{\mu}(z)$-term is forbidden by $\mathbb{Z}_2$ symmetry, we have in general $\delta\tilde{\mu}(z) \sim M(z)^2$. Furthermore, by treating derivatives to be of order $O(M(z))$ we get to fourth order

$$\begin{aligned}\Omega_{\rm GNT}/N = \Omega_{\rm unbroken} + \frac{1}{L}\int dz\Big(&\alpha_{2,0}M(z)^2 + \alpha_{4,0}(M(z)^4 + M'(z)^2) + \alpha_{2,1}M^2\delta\tilde{\mu}(z)\\ &+\alpha_{0,2}\delta\tilde{\mu}(z)^2\Big) + \ldots\end{aligned} \tag{A12}$$

and observe that the prefactors of the $M(z)^2$ and $M'(z)^2$ terms are those obtained for the GN model upon replacing $\mu \to \tilde{\mu}_0$. From this we conclude that the location of the Lifshitz point in the $\tilde{\mu} - T$ diagram is the same as in the GN model. Consequently, since the density there is directly given through $\tilde{\mu}_0$, G_V does not affect the Lifshitz point in the $\bar{n} - T$ diagram, while in the $\mu - T$ diagram the LP is shifted by $G_V\langle\bar{\psi}\gamma^0\psi\rangle/N$ in the μ-direction.

Another property that is inherited from the GN model is the second-order transition line from the chiral crystalline to the restored phase. Since in this case the magnitude of the order parameter vanishes continuously while the modulation stays finite, we have to consider the GL expansion to

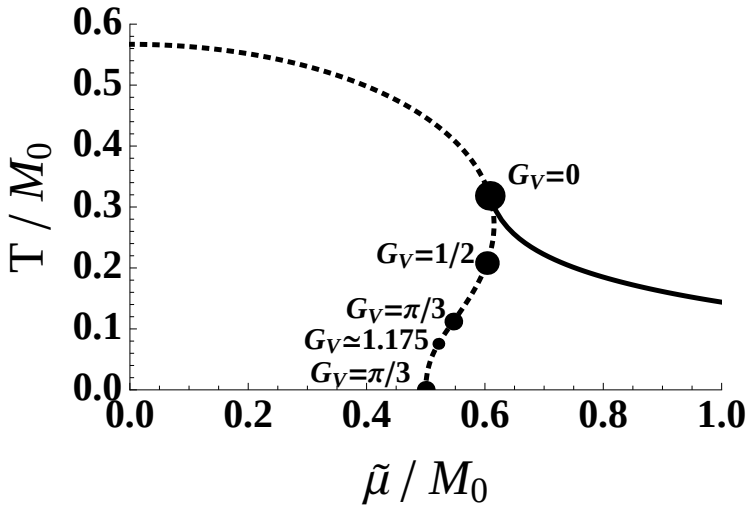

FIG. 10: Phase diagram of the massless GNT model: The dotted line corresponds to $\alpha_{2,0} = 0$, the dots indicate the critical points when limiting to homogeneous phases, i.e., in addition $\beta_4 = 0$. At $G_V = \pi/3$ an additional CP emerges on the $\tilde{\mu}$-axis, which merges with the other CP at $G_{V,\max} \simeq 1.175$. The solid line shows the transition from the chiral crystalline to the restored phase, ending at the Lifshitz point. The latter agrees with the CP at $G_V = 0$.

order $O(M(z)^2)$ and in principle to all orders of gradients. However, since $\delta\tilde{\mu}(z) \sim M(z)^2$, $\delta\tilde{\mu}$ does not enter in this analysis and we have to have the same result as in the GN model. For the latter this transition line has been determined in Refs. [36, 38] and is also depicted in Fig.(10).

[1] A. M. Halasz, A. D. Jackson, R. E. Shrock, M. A. Stephanov, and J. J. M. Verbaarschot, Phys. Rev. D **58**, 096007 (1998) [arXiv:hep-ph/9804290].

[2] M. A. Stephanov, Prog. Theor. Phys. Suppl. **153**, 139 (2004) [Int. J. Mod. Phys. A **20**, 4387 (2005)] [arXiv:hep-ph/0402115]; PoS **LAT2006**, 024 (2006) [arXiv:hep-lat/0701002].

[3] P. Braun-Munzinger and J. Wambach, Rev. Mod. Phys. **81**, 1031 (2009) [arXiv:0801.4256 [hep-ph]].

[4] Y. Nambu and G. Jona-Lasinio, Phys. Rev. **122**, 345 (1961); Phys. Rev. **124**, 246 (1961).

[5] U. Vogl and W. Weise, Prog. Part. Nucl. Phys. **27**, 195 (1991).

[6] S. P. Klevansky, Rev. Mod. Phys. **64**, 649 (1992).

[7] T. Hatsuda and T. Kunihiro, Phys. Rept. **247**, 221 (1994) [arXiv:hep-ph/9401310].

[8] M. Buballa, Phys. Rept. **407**, 205 (2005) [arXiv:hep-ph/0402234].

[9] J. D. Walecka, Annals Phys. **83**, 491 (1974).

[10] K. Fukushima, Phys. Rev. D **77**, 114028 (2008) [Erratum-ibid. D **78**, 039902 (2008)] [arXiv:0803.3318 [hep-ph]].

[11] K. Fukushima, Phys. Rev. D **78**, 114019 (2008) [arXiv:0809.3080 [hep-ph]].

[12] Z. Zhang and T. Kunihiro, Phys. Rev. D **80**, 014015 (2009) [arXiv:0904.1062 [hep-ph]].

[13] K. Fukushima, Phys. Lett. B **591**, 277 (2004) [arXiv:hep-ph/0310121].

[14] C. Ratti, M. A. Thaler and W. Weise, Phys. Rev. D **73**, 014019 (2006) [arXiv:hep-ph/0506234].

[15] B. J. Schaefer, J. M. Pawlowski and J. Wambach, Phys. Rev. D **76**, 074023 (2007) [arXiv:0704.3234

[hep-ph]].
[16] H. Abuki, M. Ciminale, R. Gatto and M. Ruggieri, Phys. Rev. D **79**, 034021 (2009) [arXiv:0811.1512 [hep-ph]].
[17] L. McLerran, K. Redlich and C. Sasaki, Nucl. Phys. A **824**, 86 (2009) [arXiv:0812.3585 [hep-ph]].
[18] L. McLerran and R. D. Pisarski, Nucl. Phys. A **796**, 83 (2007) [arXiv:0706.2191 [hep-ph]].
[19] A. S. Goldhaber and N. S. Manton, Phys. Lett. B **198**, 231 (1987).
[20] W. Broniowski, A. Kotlorz and M. Kutschera, Acta Phys. Polon. B **22**, 145 (1991).
[21] D. V. Deryagin, D. Y. Grigoriev and V. A. Rubakov, Int. J. Mod. Phys. A **7**, 659 (1992).
[22] E. Shuster and D. T. Son, Nucl. Phys. B **573**, 434 (2000) [arXiv:hep-ph/9905448].
[23] T. Kojo, Y. Hidaka, L. McLerran and R. D. Pisarski, arXiv:0912.3800 [hep-ph].
[24] M. Rozali, H. H. Shieh, M. Van Raamsdonk and J. Wu, JHEP **0801**, 053 (2008) [arXiv:0708.1322 [hep-th]].
[25] A. W. Overhauser, Phys. Rev. **128**, 1437 (1962).
[26] M. G. Alford, J. A. Bowers and K. Rajagopal, Phys. Rev. D **63**, 074016 (2001).
[27] J. A. Bowers and K. Rajagopal, Phys. Rev. D **66**, 065002 (2002).
[28] R. Casalbuoni, R. Gatto, N. Ippolito, G. Nardulli and M. Ruggieri, Phys. Lett. B **627**, 89 (2005); Erratum-ibid. B **634**, 565 (2006).
[29] M. Mannarelli, K. Rajagopal and R. Sharma, Phys. Rev. D **73**, 114012 (2006).
[30] K. Rajagopal and R. Sharma, Phys. Rev. D **74**, 094019 (2006).
[31] D. Nickel and M. Buballa, Phys. Rev. D **79**, 054009 (2009) [arXiv:0811.2400 [hep-ph]].
[32] A. Sedrakian and D. H. Rischke, Phys. Rev. D **80**, 074022 (2009).
[33] P. Fulde and R. A. Ferrell, Phys. Rev. **135**, A550 (1964).
[34] A. I. Larkin and Yu. N. Ovchinnikov, Zh. Eksp. Teor. Fiz. **47**, 1136 (1964); Sov. Phys. JETP **20** 762 (1965).
[35] D. J. Gross and A. Neveu, Phys. Rev. D **10**, 3235 (1974).
[36] O. Schnetz, M. Thies and K. Urlichs, Annals Phys. **314**, 425 (2004) [arXiv:hep-th/0402014].
[37] O. Schnetz, M. Thies and K. Urlichs, Annals Phys. **321**, 2604 (2006) [arXiv:hep-th/0511206].
[38] M. Thies, J. Phys. A **39**, 12707 (2006) [arXiv:hep-th/0601049].
[39] G. Basar, G. V. Dunne and M. Thies, Phys. Rev. D **79**, 105012 (2009) [arXiv:0903.1868 [hep-th]].
[40] M. Sadzikowski and W. Broniowski, Phys. Lett. B **488**, 63 (2000) [arXiv:hep-ph/0003282].
[41] E. Nakano and T. Tatsumi, Phys. Rev. D **71**, 114006 (2005) [arXiv:hep-ph/0411350].
[42] R. Rapp, E. V. Shuryak and I. Zahed, Phys. Rev. D **63**, 034008 (2001) [arXiv:hep-ph/0008207].
[43] D. Nickel, Phys. Rev. D **80**, 074025 (2009) [arXiv:0906.5295 [hep-ph]].
[44] D. Nickel, Phys. Rev. Lett. **103**, 072301 (2009) [arXiv:0902.1778 [hep-ph]].
[45] M. A. Stephanov, K. Rajagopal and E. V. Shuryak, Phys. Rev. Lett. **81**, 4816 (1998) [arXiv:hep-ph/9806219].
[46] F. Correa, G. V. Dunne and M. S. Plyushchay, Annals Phys. **324**, 2522 (2009) [arXiv:0904.2768 [hep-th]].
[47] D. Ebert and H. Reinhardt, Nucl. Phys. B **271**, 188 (1986).
[48] M. Buballa, Nucl. Phys. A **611**, 393 (1996) [arXiv:nucl-th/9609044].
[49] M. Kitazawa, T. Koide, T. Kunihiro and Y. Nemoto, Prog. Theor. Phys. **108**, 929 (2002) [arXiv:hep-ph/0207255].
[50] L. D. McLerran, B. Svetitsky, Phys. Rev. **D24**, 450 (1981).
[51] F. Karsch, H. W. Wyld, Phys. Rev. Lett. **55**, 2242 (1985).
[52] S. Rößner, C. Ratti and W. Weise, Phys. Rev. D **75**, 034007 (2007).
[53] L. D. Landau and E. M. Lifshitz, Statistical physics (Addison-Wesley, Reading, Mass., 1969)

[54] G. Baym, B. L. Friman and G. Grinstein, Nucl. Phys. B **210**, 193 (1982)
[55] C. Boehmer, M. Thies and K. Urlichs, Phys. Rev. D **75**, 105017 (2007) [arXiv:hep-th/0702201].